

Statespecific unimolecular reaction of NO₂ just above the dissociation threshold

Jun Miyawaki, Kaoru Yamanouchi, and Soji Tsuchiya

Citation: *The Journal of Chemical Physics* **99**, 254 (1993); doi: 10.1063/1.465802

View online: <http://dx.doi.org/10.1063/1.465802>

View Table of Contents: <http://scitation.aip.org/content/aip/journal/jcp/99/1?ver=pdfcov>

Published by the [AIP Publishing](#)

Articles you may be interested in

[Semiclassical modeling of state-specific dissociation rates in diatomic gases](#)

J. Chem. Phys. **113**, 7351 (2000); 10.1063/1.1313386

[Statespecific unimolecular dissociation dynamics of HFCO. II. CO rotational distribution and Doppler widths](#)

J. Chem. Phys. **103**, 9981 (1995); 10.1063/1.469887

[Response to "Comment on 'Statespecific unimolecular reaction of NO₂ just above the dissociation threshold'" \[J. Chem. Phys. 100, 4714 \(1994\)\]](#)

J. Chem. Phys. **100**, 4716 (1994); 10.1063/1.466262

[Comment on "Statespecific unimolecular reaction of NO₂ just above the dissociation threshold" \[J. Chem. Phys. 99, 254 \(1993\)\]](#)

J. Chem. Phys. **100**, 4714 (1994); 10.1063/1.466261

[Statespecific unimolecular reaction dynamics of HFCO. I. Dissociation rates](#)

J. Chem. Phys. **97**, 1010 (1992); 10.1063/1.463280



State-specific unimolecular reaction of NO₂ just above the dissociation threshold

Jun Miyawaki, Kaoru Yamanouchi, and Soji Tsuchiya

Department of Pure and Applied Sciences, College of Arts and Sciences, The University of Tokyo, Komaba, Meguro-ku, Tokyo 153, Japan

(Received 24 December 1992; accepted 16 March 1993)

Photofragment excitation (PHOFEX) spectra of NO₂ are observed by monitoring the specific quantum states of a fragment NO (²Π_{1/2}; *v*=0, *J*=0.5–6.5) in the energy region 0–160 cm⁻¹ above the dissociation limit to NO (²Π_{1/2}) and O (³P₂). Preparation of NO₂ in a quasibound eigenstate above the dissociation limit is attained by the combination of extremely cooled (~1 K) parent NO₂ in a supersonic jet and a high resolution (~0.05 cm⁻¹) photolysis laser. The dissociation rate constants are obtained from the peak width of PHOFEX spectra and the smallest rate constant is *k*=8.5×10⁹ s⁻¹, in the energy region where only *J*=0.5 of NO (²Π_{1/2}; *v*=0) is produced. The observation that the rate constant increases stepwise when a new product channel *J*=1.5 opens implies that the transition state is a loose complex. This behavior of the rate constant is direct experimental proof of the statistical theory of the unimolecular reaction process. The product state distribution of NO fluctuates depending on the quasibound state of NO₂, though the average value is consistent with the calculation by phase space theory. This state specificity of the rate constant is interpreted in terms of quantum fluctuations associated with individual quasibound eigenstates.

I. INTRODUCTION

In recent years, investigations of the unimolecular dissociation reaction process of polyatomic molecules selectively excited in a specific vibrational mode have attracted great interest,¹ since it may answer the key question of how fast is the intramolecular vibrational energy redistribution (IVR) on a chemically significant time scale. If IVR occurs very fast and finishes before the dissociation reaction, the unimolecular reaction may proceed statistically, as predicted by statistical theories.² If it does not, a mode-specific unimolecular reaction may be realized. By application of recent laser techniques, it becomes possible to prepare a molecule in a certain selected eigenstate, and thus large numbers of experiments have been performed to look for such a mode-specific reaction.

The mode specificity of a unimolecular reaction may be identified through observation of the dependence of the reaction rate or the product state distribution on a well-characterized initially excited level of the parent molecule. Several examples of state-specific photodissociation reactions have been reported so far,^{3–6} but it is not always clear how these state specificities are related to the vibrational mode (or modes) of the parent molecule. To our knowledge, the clearest observation of vibrational-mode specificity is that reported by Choi and Moore⁵ on the photodissociation of HFCO. They measured the dissociation rate constants of HFCO in quasibound highly excited vibrational levels in the S₀ state, prepared by stimulated emission pumping. The HFCO molecules in vibrational levels with high excitation in the out-of-plane bending mode (*v*₆) dissociate more slowly than those in other energetically adjacent levels. This is interpreted as being caused by the *v*₆ mode being uncoupled from other vibrational modes,

and the state specificity is ascribed to the incompleteness of the mode couplings.

Recently, another explanation for observed state specificity was proposed by Polik *et al.*^{7,8} and Miller *et al.*⁹ Polik *et al.* measured the Stark-level crossing spectra of D₂CO in the energy region above the dissociation barrier and derived the dissociation rate constants of D₂CO in rovibrational eigenstates in the 28 300 cm⁻¹ region of the electronic ground S₀ state.⁷ The observed rate constants for these respective S₀ levels fluctuate within three orders of magnitude, though the averaged rate constant is in accord with the Rice–Ramsperger–Kassel–Marcus (RRKM) theory including a tunneling correction. Based on the distribution of the observed level spacings and from estimated S₁–S₀ coupling matrix elements, the fluctuation of the observed rate constants over a wide range is interpreted as a quantum statistical fluctuation which is a necessary consequence of the complete mixing of vibrational modes.^{8,9}

In order to investigate a state-specific reaction, it is necessary to excite the relevant molecules to a specific eigenstate. In the present study, we have investigated the state-selected photodissociation of NO₂, NO₂→NO (²Π_Ω; Ω=1/2,3/2) + O (³P_{*j*}; *j*=2,1,0). The state-selective preparation of NO₂ in its quasibound states is possible through internal conversion. It is well known that the strong vibronic coupling between the electronic excited state ²B₂ and the electronic ground state ²A₁ causes a formidable complexity of the absorption spectrum even in the energy region much below the photodissociation limit,¹⁰ i.e., one vibronic state in the ²B₂ state couples with a large number of highly excited vibrational states in the electronic ground ²A₁ state resulting in many eigenstates with ²B₂ character. This strong vibronic coupling also causes a complicated structure in the absorption spectrum in the UV region beyond the dissociation limit, above which the

quantum yield for fluorescence approaches zero. Thus, it is possible to prepare NO₂ through the ${}^2B_2\text{-}{}^2A_1$ transition in a quasibound state whose energy exceeds the dissociation threshold.

Regarding the photodissociation studies of NO₂, Zacharias *et al.* observed a product state distribution of the NO fragment in photolysis at 337 (Ref. 11), 351, and 308 nm (Ref. 12) and found that NO is highly vibrationally excited and its vibrational population distribution is an inverted one. Mons and Dimicoli¹³ observed the rotational distribution of NO ($\nu=1$) produced from the photodissociation of thermal NO₂ at 370, 365, 361, and 348 nm, and the rotational distributions are well described by a prior distribution. On the other hand, very recently Robie *et al.*¹⁴ observed the rotational distribution of NO ($\nu=1$) at two photolysis wavelengths around 369 nm using NO₂ cooled in a supersonic jet and found that the rotational distributions are well explained by phase space theory (PST), though a fluctuation around the theoretical estimates is observed.

Just above the dissociation limit (~ 397 nm), Robra *et al.*¹⁵ observed the photofragment excitation (PHOFEX) spectrum of NO₂ by monitoring NO (${}^2\Pi_{1/2}; \nu=0, J=0.5\text{-}7.5$). In their PHOFEX spectra, a certain variation of intensities is observed and this structure is sensitively dependent on the monitored level of the NO fragment. The former fact indicates the existence of quasibound levels above the dissociation limit and the latter indicates that the product state distribution is state specific. In a previous study, we observed the PHOFEX spectrum by monitoring the other fragment, atomic oxygen O (${}^3P_j; j=0, 1, \text{ and } 2$) near the dissociation limit.¹⁶ State specificity was also observed as a fluctuation of the population ratio of spin-orbit sublevels of O (3P_j).

In the present study, in order to prepare a single rovibrational eigenstate as an initial state of a unimolecular reaction, NO₂ is prepared rotationally ultracold and a high resolution laser is employed as the photolysis light source. We measure the PHOFEX spectrum of NO₂ just above the dissociation limit by monitoring NO in specific quantum states. The fact that the dissociation rate increases stepwise when the new product state is energetically allowed justifies the statistical theory. A state-dependent product state distribution which fluctuates around the value expected by the statistical theory is observed and this is interpreted as a statistical fluctuation due to the complete mixing of vibrational modes in NO₂.

II. EXPERIMENT

In the measurements of laser-induced fluorescence (LIF) and PHOFEX spectra near the dissociation threshold region, rotationally cold NO₂ is prepared in a supersonic jet which is formed by expansion of a NO₂ (0.2%)/He mixture with a stagnation pressure of 5 atm into a vacuum chamber through a pulsed nozzle (General Valve 9-279-900) with an orifice diameter of 0.8 mm.

Two dye lasers (Lambda Physik FL3002E) are simultaneously excited by a XeCl excimer laser (Lambda Physik EMG101MSC). One dye laser output (~ 400 nm) is used

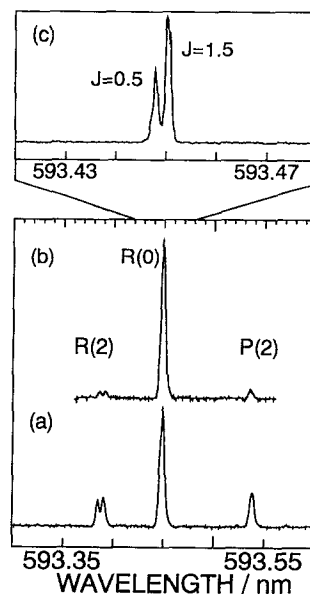


FIG. 1. (a) and (b) The low resolution and (c) high resolution LIF spectra of NO₂ ~ 593 nm. The gas mixtures used are (a) 5% NO₂/He and (b) and (c) 0.2% NO₂/He.

to excite and photolyze NO₂ and the output of the other is frequency doubled (~ 226 nm) by a β -BBO crystal and is used to monitor the NO fragment. The resolution of both lasers is 0.5 cm^{-1} in the low resolution measurements. In the high resolution measurements, a resolution of 0.05 cm^{-1} is attained for the excitation laser by using an intracavity etalon.

The photolysis laser beam and the monitor laser beam collinearly counterpropagate and perpendicularly cross the jet 32 mm downstream from the nozzle orifice. The monitor laser beam is optically delayed by 10 ns from the photolysis laser. The polarizations of both laser beams are usually perpendicular to each other. When polarization effects are measured, the polarization of the probe laser is rotated by a Fresnel-Rhomb retarder. The photofragment NO from NO₂ is detected by measuring the LIF signal of the $A({}^2\Sigma)\text{-}X({}^2\Pi_{1/2})$ transitions. The fluorescence is collected by a solar-blind photomultiplier (Hamamatsu R166UH) placed in a direction perpendicular to both the laser beam and the jet axis. The signal is amplified by a preamplifier (NF BX-31) and averaged by a boxcar integrator (Stanford SR250). In order to record a PHOFEX spectrum of NO, the wavelength of the photolysis laser is scanned by fixing the monitor laser wavelength at each of the $A\text{-}X$ vibration-rotation transitions of NO. The product state distribution of NO is derived from the LIF spectrum of NO produced at a certain fixed wavelength of the photolysis laser.

In order to estimate the rotational temperature, we observed rotational structure of the NO₂ band at 593 nm, which has been assigned to the ${}^2B_2\text{-}{}^2A_1$ ($K=0\leftarrow K=0$) transition by Smalley *et al.*¹⁷ As is shown in Fig. 1, the rotational structure is composed of almost one peak, i.e., the R(0) transition. The rotational temperature is derived to be about 0.9 K, at which almost all NO₂ (98%) mole-

cules are in the 0₀₀ rotational level and the concentration of rotationally hot NO₂ in the 2₀₂ level is only 2%. Since the NO₂ molecule has an electron spin angular momentum of $S=1/2$, the $R(0)$ transition has two fine-structure components $J=1/2$ and $J=3/2$. When the spectrum is measured with high resolution (0.05 cm^{-1}), these two components can be observed separately.

The concentration of N₂O₄ in the 0.2% NO₂/He mixture (5 atm total pressure) at room temperature is estimated to be 6% from the equilibrium constant for the dimerization reaction of NO₂. However, its contribution to the spectra can be neglected because (i) the absorption cross section of N₂O₄ in the visible and UV regions above 380 nm is $10\text{--}10^2$ times smaller than that of NO₂ (Ref. 18), and (ii) even if N₂O₄ absorbs a photon at wavelength around 400 nm, its energy is insufficient for the photodissociation of N₂O₄.¹⁹

Since the dissociation threshold of NO₂ is clearly identified in the LIF and PHOFEX spectra in the present study (see Sec. III B), the threshold can be used as a wavenumber standard in the spectra. However, two slightly different values have been reported for the threshold energy of the dissociation $\text{NO}_2 \rightarrow \text{NO} (^2\Pi_{1/2}) + \text{O} (^3P_2)$, i.e., $25\,130.6 \pm 0.6\text{ cm}^{-1}$ by Robra *et al.*¹⁵ and $25\,128.5 \pm 0.2\text{ cm}^{-1}$ by Butenhoff and Rohlfiing.²⁰ Thus, in the present study, only the relative wavenumber measured from the dissociation limit of NO₂, i.e., the excess energy, is used in the discussion as well as in figures. In the high resolution measurements, the linearity of the wavenumber is assured by monitoring the fringe pattern of a monitor etalon.

III. RESULTS

A. PHOFEX spectra for NO(J) ($J=0.5\text{--}6.5$)

Above its first dissociation limit, NO₂ dissociates to NO ($^2\Pi_{1/2}$) and O (3P_2). The relative energies of the spin-orbit sublevels O (3P_0) and O (3P_1) measured from the lowest sublevel O (3P_2) are 226.5 and 158.5 cm^{-1} , respectively.²¹ The $v=0$ level of NO ($^2\Pi_{3/2}$) is higher in energy by 119.7 cm^{-1} than that of NO ($^2\Pi_{1/2}$).²²

In the low resolution measurement of PHOFEX spectra, NO ($^2\Pi_{1/2}; v=0, J=0.5\text{--}6.5$) is monitored. Since the wavenumber of the excess energy is varied between $0\text{--}160\text{ cm}^{-1}$, the counterpart fragment O is limited to O (3P_2). Each rotational level of NO ($^2\Pi_{1/2}$) has two Λ doublet components A' and A'' and the splitting of these two components ($<0.01\text{ cm}^{-1}$) is smaller than the laser resolution. However, each component can be detected selectively by choosing the rotational branches of the NO $A (^2\Sigma) \rightarrow X (^2\Pi_{1/2})$ transition.

The PHOFEX spectra obtained by detecting NO ($J=0.5\text{--}6.5$) are shown in Fig. 2. The resolution of the photolysis laser is about 0.5 cm^{-1} and the rotational temperature of the parent NO₂ is 0.9 K. Apart from small differences in the resolution of the photolysis laser and the rotational temperature of NO₂, our data are consistent with the results reported by Robra *et al.*¹⁵ which were obtained for NO₂ with a rotational temperature of 2.5 K and with a laser resolution of 0.2 cm^{-1} . Within the resolution

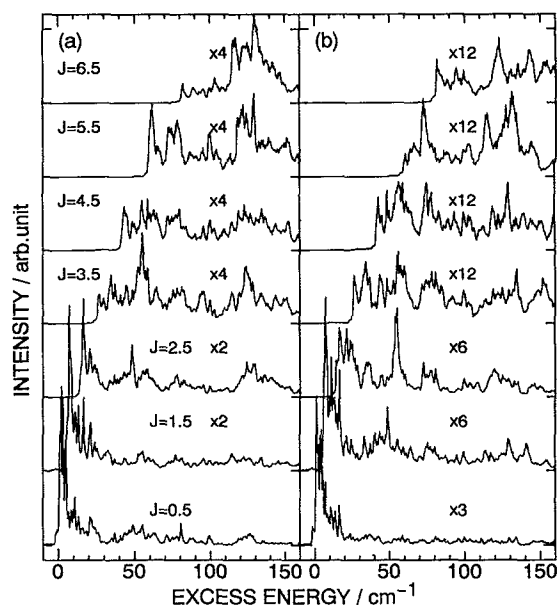


FIG. 2. The PHOFEX spectra of NO₂ obtained by monitoring fragment NO ($^2\Pi_{1/2}; v=0, J=0.5\text{--}6.5$) in the excess energy range between -10 and 160 cm^{-1} . The spectra for the Λ doublet components of A' and A'' are shown in (a) and (b), respectively. The resolution of the photolysis laser is about 0.5 cm^{-1} .

of the photolysis laser, the threshold energy for each rotational level of NO agrees well with that calculated from the rotational constant of a free NO molecule.²² This implies that there is no barrier along the dissociation reaction coordinate on the potential energy surface (see Sec. IV A). As seen clearly in Fig. 2, intensity patterns of the PHOFEX spectra for respective J levels of the product NO are considerably different from each other. This means that the product state distribution changes significantly depending on the photolysis energy.

B. LIF and PHOFEX spectra near the dissociation threshold

Shown in Fig. 3 are the LIF spectrum of NO₂ below the dissociation limit and the PHOFEX spectrum obtained

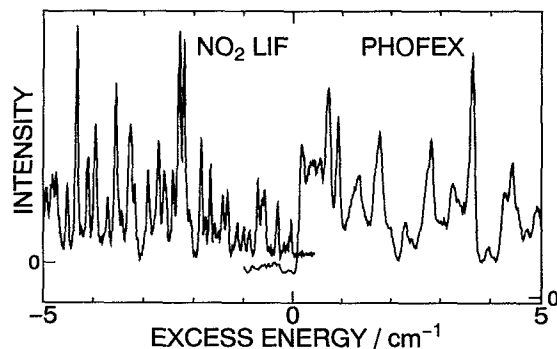


FIG. 3. The high resolution LIF spectrum of NO₂ below the dissociation threshold and the PHOFEX spectrum of NO₂ above the dissociation threshold observed by monitoring the A'' component of NO ($^2\Pi_{1/2}; v=0, J=0.5$). The FWHM of the peaks in the LIF spectrum is about 0.055 cm^{-1} .

by monitoring NO ($J=0.5$) above the dissociation limit. Both spectra are taken with the high resolution excitation laser. In this figure, the dissociation threshold is clearly identified, i.e., as the excitation wavenumber is scanned towards higher energy, the LIF signal disappears suddenly at the dissociation threshold and the PHOFEX signal starts to emerge. The small contribution of rotationally hot NO₂ is seen in the PHOFEX spectrum just below the dissociation threshold. The observed linewidths of isolated peaks in the LIF spectrum below the dissociation threshold are all about 0.055 cm^{-1} and this value is regarded as the resolution of the excitation laser for the high resolution LIF and PHOFEX measurements in this region. The number of peaks identified in the whole energy region of the LIF spectrum between -5.0 and 0.0 cm^{-1} is 41. Thus, the average density of peaks is derived to be 8.2 peaks/cm^{-1} just below the dissociation limit. As explained in Sec. II, two peaks correspond to the transition to one vibronic level, so that the estimated density of vibronic levels is about $4.1\text{ levels/cm}^{-1}$. However, the density of vibrational levels in this energy region of the 2B_2 electronic state is expected to be smaller than this value by two orders of magnitude. Therefore, it is obvious that the observed peaks represent the transitions to levels formed by vibronic coupling of the 2B_2 vibronic levels with highly excited vibrational levels in the electronic ground 2A_1 state.

Although there is spectral structure in the PHOFEX spectrum which may indicate the existence of discrete states, the linewidth of each peak in the PHOFEX spectrum is considerably broader than that in the LIF spectrum and the density of peaks per cm^{-1} in the PHOFEX spectrum (3.4 peaks/cm^{-1}) is considerably smaller than that of the LIF spectrum (8.2 peaks/cm^{-1}). It is reasonable to interpret that the level structure in the PHOFEX spectrum is basically the same as that in the LIF spectrum, i.e., NO₂ predissociates through its quasibound levels above the dissociation limit and the homogeneous line broadening is due to the predissociation. The smaller density of states in the PHOFEX spectrum compared with the LIF measurements is thought to be due to considerable overlapping of the broadened peaks.

When the photolysis energy exceeds the dissociation threshold by 5.0 cm^{-1} , the second lowest dissociation channel producing the rotational level of $J=1.5$ opens. In Fig. 4(a), two PHOFEX spectra of $J=0.5$ and $J=1.5$ for the A' component of the Λ doublet are shown, and in Fig. 4(b) those for the A'' component are shown. In the energy region where only $J=0.5$ is produced, the widths of the observed peaks are relatively narrow, but in the energy region where both of the two channels $J=0.5$ and 1.5 are energetically allowed, such narrow peaks disappear. In other words, the peak width becomes larger suddenly when the new product channel ($J=1.5$) opens.

In Fig. 5, the observed peak width Γ [full width at half-maximum (FWHM)] is plotted against the photolysis energy. In the region where only the $J=0.5$ channel is open, it is possible to identify several relatively isolated peaks whose widths are $\sim 0.1\text{ cm}^{-1}$. These peaks are then fitted by a Lorentzian function. The homogeneous peak

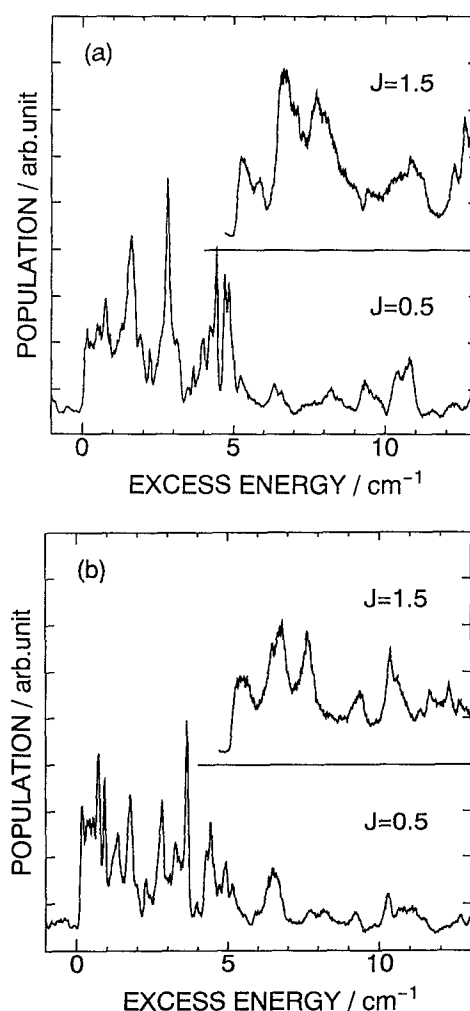


FIG. 4. The PHOFEX spectra for $J=0.5$ and 1.5 of NO. The Λ doublet components of A' and A'' are shown in (a) and (b), respectively. The threshold $5.01 \pm 0.05\text{ cm}^{-1}$ for the NO $J=1.5$ spectrum coincides with the rotational energy 5.015 cm^{-1} of the $J=1.5$ level of free NO.

width, i.e., the broadening due to the predissociation is obtained by subtracting the FWHM (0.055 cm^{-1}) of the LIF spectral peaks just below the dissociation threshold from the observed linewidth. The peakwidth Γ can be converted to a dissociation rate constant k by using the relationship $\Gamma = k\hbar$, where \hbar is Planck's constant. Deconvolution of the whole spectrum is impossible because of the overlapping of two or more peaks and the lack of knowledge on the positions of these peaks, but in the region where only $J=0.5$ is produced, the linewidths are derived only for isolated peaks from the fitting to a Lorentzian line shape by disregarding the effect of superposition of tails of adjacent peaks. It is also possible that several overlapping peaks form one peak, especially in the case of the broader peaks. Thus, the derived estimates of the linewidth give an upper bound. The smallest rate constant derived from the upper bounds of the peak widths is $8.5 \times 10^9\text{ s}^{-1}$.

C. Product state distribution

At several fixed photolysis wavenumbers, the rotational structure of the LIF spectra of the fragment NO is

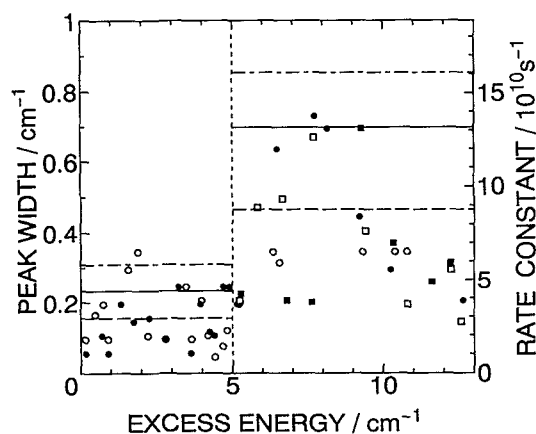


FIG. 5. The peak width of PHOFEX spectra in Fig. 3 as a function of the excess energy. The A' (open circle) and A'' (filled circle) of $J=0.5$ and A' (open square) and A'' (filled square) of $J=1.5$ are shown. The vertical broken line at 5.015 cm^{-1} represents the threshold for $J=1.5$. Calculated values by using PST are also shown for $J_{\text{NO}_2}=0.5$ (dashed line), 1.5 (dotted-dashed line), and the complete K -mixing case (solid line).

observed to obtain a rotational state distribution. For example, in Fig. 6(a), the rotational state distribution at an excess energy of 88 cm^{-1} is plotted as a function of J for both components of the Λ doublet. Though the populations of both components A' and A'' vary significantly when J changes, their dependence on J is different for A' and A'' and no correlation is found between them. The J dependencies of the A' and A'' components are completely different when the photolysis wavenumber changes, as shown in Fig. 6(b), where the rotational state distribution obtained at an excess energy of 124 cm^{-1} is shown.

The measurements of the LIF spectra of NO are used for intensity normalization of the PHOFEX spectra shown in Fig. 2. These PHOFEX spectra are measured separately with the wavenumber of the probe laser fixed at a particular rotational transition of NO. Thus, by the measurements of the produced NO at several photolysis wavelengths and by taking into account the Hönl-London factors of each transition, PHOFEX spectra are converted so that they represent the relative population. Due to experimental errors in the intensities of the PHOFEX spectra ($\pm 10\%$) and the LIF spectra of NO ($\pm 10\%$), the de-

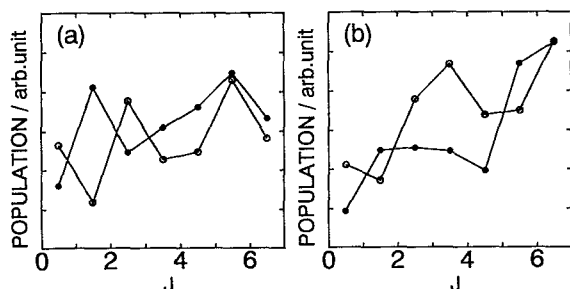


FIG. 6. The rotational state distributions of NO at the excess energies of (a) 88 and (b) 124 cm^{-1} . Open and filled circles represent A' and A'' components of the Λ doublet, respectively.

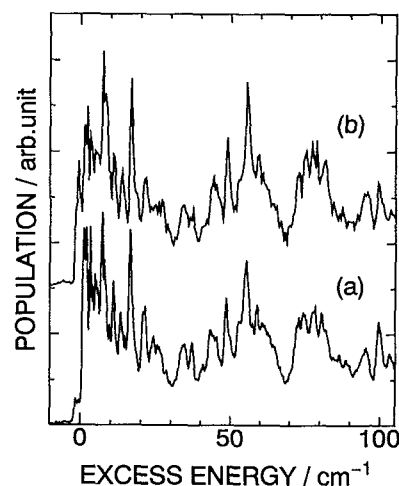


FIG. 7. (a) The summation of the populations of NO in the $J=0.5-6.5$ levels for both of the Λ doublet components. (b) The PHOFEX spectrum of O (3P_2) (Ref. 16).

rived population of NO for a particular J of each Λ doublet component has an experimental error of $\pm 15\%$. The summation of population for each J and Λ doublet component of NO should be equal to the population of the other fragment O (3P_2). In Fig. 7, the total sum of NO populations [Fig. 7(a)] is compared with the PHOFEX spectrum of O (3P_2) (Ref. 16) [Fig. 7(b)]. They agree well with each other within their experimental errors.

In Fig. 8, the fraction of the population in the A' component $P(A')/[P(A') + P(A'')]$ is plotted for $J=0.5-6.5$ as a function of the photolysis energy. The observed fractions fluctuate considerably and no correlation is found among these oscillatory patterns. However, it is interesting to note that if the fraction is averaged over a wide energy region,

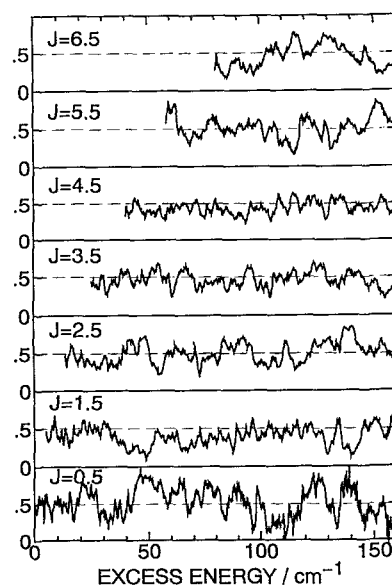


FIG. 8. The fraction of the A' component $P(A')/[P(A') + P(A'')]$ for $J=0.5-6.5$.

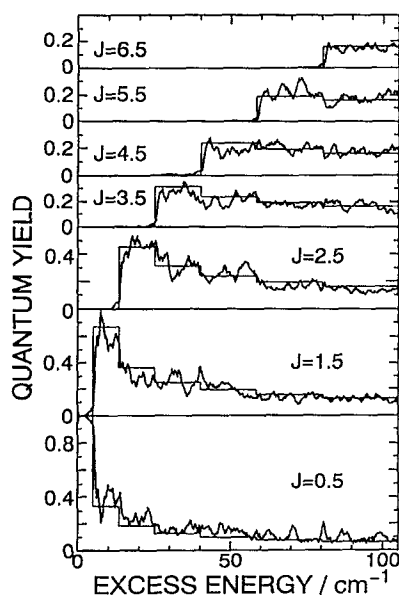


FIG. 9. The quantum yield for NO $J=0.5-6.5$. The two Λ doublet components of each J are averaged. The staircase line represents an expected value calculated by PST.

the average value converges to 0.5 within the experimental error.

Although the relative population in each J and Λ doublet component fluctuates considerably, this fluctuation becomes smaller when the two Λ doublet components having the same J are averaged. Figure 9 shows the quantum yield of NO(J) and that calculated by phase space theory (PST) (see Sec. IV C). The calculated quantum yield depicted by horizontal bars in Fig. 9 agrees well with the overall pattern of the observed population ratios, but there is also some fluctuation around the expected value.

Using the population ratios shown in Fig. 9, the energy partitioned to rotation of NO, E_{rot} , is calculated as

$$E_{\text{rot}} = \frac{\sum n(J) E_{\text{rot}}(J)}{\sum n(J)}, \quad (1)$$

where $n(J)$ represents the relative population of NO(J) averaged over the two components of the Λ doublet. E_{rot} derived from Eq. (1) is drawn in Fig. 10. It is shown

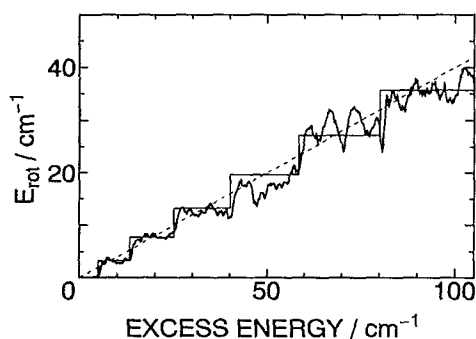


FIG. 10. The energy partitioned in rotation of NO against the excess energy. The staircase line represents an expected value calculated by PST. The broken line represents $E_{\text{rot}} = 0.40 \times (\text{excess energy})$.

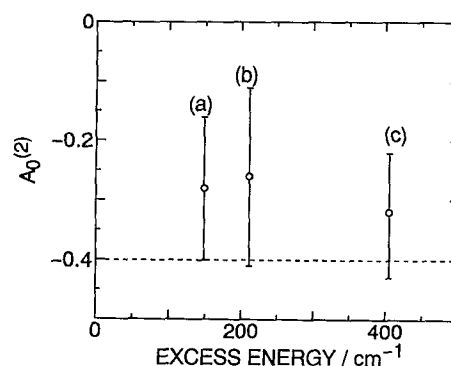


FIG. 11. The rotational alignment parameter $A_0^{(2)}$. The ${}^5R(6.5)$ transition is used in (a) and (b), and the ${}^5R(8.5)$ transition is used in (c).

clearly that E_{rot} increases stepwise as each new rotational level of NO becomes energetically allowed. The photolysis energy dependence of E_{rot} is in good agreement with the PST prediction as compared in this figure. The slope of E_{rot} vs excess energy shows that the energy partitioned to the rotational degree of freedom is about 40% of the total excess energy and the value is consistent with the value of $42\% \pm 5\%$ derived by Robra *et al.*¹⁵ within the experimental errors.

D. Polarization effect

The rotational alignment parameter $A_0^{(2)}$ is obtained from the dependence of the LIF intensity on the polarization of the probe laser. In the analysis, we followed the treatment by Greene and Zare.²³ In their treatment, the LIF intensity (I) is given by

$$I = CS \sum A_0^{(k)}(J) \epsilon(k_d, k_a, k, 0; \Omega) \omega(k_d, k_a, k; J_i, J_e, J_f), \quad (2)$$

where C is a constant proportional to the total population of the initial state, S is the product of line strengths for absorption and emission processes, ϵ represents a geometrical factor depending on the experimental setup, and ω is the angular momentum coupling factor for the LIF process. The parameter $A_0^{(k)}$ is the k th multipole moment of the angular momentum distribution in the laboratory-fixed frame for a cylindrically symmetric system around a Z axis which is defined by the electric vector of the photolysis laser. The J alignment of the fragment is depolarized by the presence of a hyperfine structure due to the nuclear spin of the N atom ($I=1$). Since the effective J alignment is reduced due to the precession of \mathbf{J} around \mathbf{F} ($=\mathbf{J}+\mathbf{I}$), the alignment factor is reduced especially at low J 's. The parameter $A_0^{(2)}$ is derived, taking into account this dealignment effect.

In Fig. 11, the derived rotational alignment parameter $A_0^{(2)}$ is plotted at three excess energies of 147, 212, and 406 cm^{-1} . The observed values are all ~ -0.3 , regardless of the photolysis energy and the total angular momentum J of NO. Generally, it is well known that the range of $A_0^{(2)}$ is $-0.4 < A_0^{(2)} < 0.8$, where $A_0^{(2)} = -0.4$ corresponds to the limit of $\mu \perp \mathbf{J}$, and 0.8 corresponds to the limit of $\mu \parallel \mathbf{J}$.

The observed negative value of $A_0^{(2)} \sim -0.3$ implies that \mathbf{J} is nearly perpendicular to $\boldsymbol{\mu}$, i.e., $\boldsymbol{\mu} \perp \mathbf{J}$. In the case of the dissociation of a triatomic molecule, the direction of the angular momentum \mathbf{N} of a diatomic fragment is perpendicular to the molecular plane when $\mathbf{J} \sim \mathbf{N}$.²⁴ As a consequence, the observed value of $A_0^{(2)}$ indicates that $\boldsymbol{\mu}$ is almost completely in the molecular plane. Since $\boldsymbol{\mu}$ for the ${}^2B_2 \rightarrow {}^2A_1$ transition lies along the a axis in the molecular plane, it can be said that NO₂ is initially excited mainly to the 2B_2 state.

The observed value of $A_0^{(2)}$ is larger than the limiting value of $A_0^{(2)} = -0.4$. There are two possible sources which reduce the degree of the rotational alignment:

(1) If the transition dipole $\boldsymbol{\mu}$ is not exactly parallel to the molecular plane, $A_0^{(2)}$ may deviate from the limit value of -0.4 . It is expected that ${}^2B_1 \rightarrow {}^2A_1$ transitions are also located in this energy region. The transition dipole $\boldsymbol{\mu}$ of the ${}^2B_1 \rightarrow {}^2A_1$ transition is perpendicular to the molecular plane. Assuming that this is the main reason for the depolarization, the fraction of the transition to 2B_1 is estimated to be about 10%, which should be regarded as an upper limit. However, this may not be the only reason for the depolarization since the contribution of the ${}^2B_1 \rightarrow {}^2A_1$ transition in this region is considered to be quite small.¹⁵

(2) When the excited NO₂ has a long dissociation lifetime compared with its rotational period it can rotate before dissociation, and the correlation between the initially aligned $\boldsymbol{\mu}$ and \mathbf{J} is broken to some extent. In the present case, NO₂ is excited to the $N_{KaKc} = 1_{01}$ rotational level, and the time required to rotate once is estimated to be about $[2cB \sqrt{N(N+1)}]^{-1} = 28$ ps, where the rotational constant $B = 0.423$ cm⁻¹ is used. If this rotation of NO₂ before the dissociation process is the main reason for the deviation of $A_0^{(2)}$ from the limiting value -0.4 , the lifetime of NO₂ can be estimated to be about 10 ps. Considering the incompleteness of the polarization of the photolysis and monitor laser light, the lifetime of about 10 ps should be regarded as an upper limit. The lifetimes estimated from the peak widths just above the dissociation limit are about 120 ps in the region where only $J=0.5$ is energetically allowed, and increase suddenly when the new product channel $J=1.5$ opens. If the rate constant increases proportionally with the number of states counted by PST, and 120 ps is used for the lifetime in the region where only $J=0.5$ is open, the rate constants at 147, 212, and 406 cm⁻¹ of the excess energies are 4.3, 3.0, and 1.9 ps, respectively. These values are in good agreement with those reported by Brucker *et al.*,²⁵ i.e., 5, 2.5, and 1.9 ps at excess energies of 60, 150, and 270 cm⁻¹, respectively. The lifetimes estimated by PST as well as those derived by Brucker *et al.* are all consistent with the upper limit of about 10 ps derived from $A_0^{(2)}$.

IV. DISCUSSION

A. Product state counting by phase space theory

Phase space theory (PST)²⁶ is the most reliable statistical theory to predict the product state distribution (PSD) in a unimolecular reaction assuming statistical partitioning

of the energy among product states. In this theory, it is assumed that all possible states are realized with equal probability provided that the total energy and the total angular momentum are conserved.

In the photodissociation process of NO₂, the conservations of total energy and total angular momentum are expressed as

$$E_{\text{NO}_2} = D_{\text{O}}(\text{ON-O}) + E_{\text{NO}}(J) + E_{\text{O}}({}^3P_2) + E_{\text{trans}}, \quad (3)$$

$$J_{\text{NO}_2} = J_{\text{NO}} + J_{\text{O}} + L, \quad (4)$$

where J_{NO_2} , J_{NO} , and J_{O} represent the total angular momenta of NO₂, NO, and the oxygen atom, respectively. Hereafter J_{NO} is simply represented as J . E_{NO_2} is the total energy given to NO₂, $D_{\text{O}}(\text{ON-O})$ is the dissociation energy, $E_{\text{NO}}(J)$ and $E({}^3P_2)$ are internal energies of NO(J) and O(3P_2), respectively, and E_{trans} is the relative translational energy of the two fragments. In the present case, the internal energy of the oxygen atom is set to zero, i.e., $E({}^3P_2) = 0$, $J_{\text{O}} = 2$, and $J_{\text{NO}_2} = 1/2$ or $3/2$ is selected as the initial level.

The maximum value of the energetically allowed orbital angular momentum L_{max} is determined from the centrifugal barrier formed by the orbital angular momentum between NO and O. If a dispersion type attractive potential $V(r) = -C_6/r^6$ is assumed as a long range attractive potential between the two fragments, this restriction is expressed as

$$2L(L+1) \leq 3\mu(2C_6)^{1/3} E_{\text{trans}}^{2/3}, \quad (5)$$

where μ is the reduced mass of the two fragments NO and O. When C_6 is extremely large, the range of L is mainly determined by the angular momentum conservation expressed in Eq. (4). If C_6 is very small, the centrifugal barrier increases as L increases and thus the dissociation threshold for $L(>0)$ is somewhat larger than that for $L=0$. Since the threshold for (J, L) , $E_{\text{th}}(J, L)$, is expressed as

$$E_{\text{th}}(J, L) = E_{\text{th}}(J, 0) + 2[2L(L+1)/6]^{3/2}/C_6^{1/2}, \quad (6)$$

C_6 can be obtained by the energy difference between the two thresholds for (J, L) and $(J, 0)$. For the precise estimation of C_6 , it is required to use the threshold for larger L . Because of the conservation of total angular momentum of the system, the largest L can be realized for the largest J . There are six thresholds in the PHOFEX spectrum of $J=6.5$, which is the largest J available in the present study, corresponding to $L=4, 5, \dots, 9$. The lowest threshold of $L=4$ is most clearly observed in the PHOFEX spectrum, but thresholds for other L are not clear due to the intensity variation in the spectra originating from the Franck-Condon absorption profile. It is found that the observed threshold, which corresponds to that for $L=4$, coincides with the calculated threshold without a centrifugal barrier ($L=0$) within the resolution (0.5 cm⁻¹) of the photolysis laser. By use of Eq. (6) and $L=4$, C_6 is estimated to be $C_6 \geq 7.8 \times 10^{-79}$ J m⁶. By using the lower bound of C_6 , the upper bound of the centrifugal barrier for $L=9$ is calcu-

lated to be $\sim 4 \text{ cm}^{-1}$. However, it is difficult to find a staircase-like change associated with such a barrier in the PHOFEX spectra due to the complicated Franck–Condon intensity pattern. The lower limit of C_6 we obtain does not contradict the value of $C_6 = 10^{-76} \text{ J m}^6$ reported by Robie *et al.*¹⁴ In their study, there is no evidence for the existence of a centrifugal barrier, since all energetically possible J_{NO} 's in an asymptotic limit are realized even for $J_{\text{NO}} \sim 30$. Thus, in the calculation of population in each rotational state of NO by PST, the restriction [Eq. (5)] is not taken into account by assuming that C_6 is large enough.

B. Dissociation rate constant

As explained in Sec. III B, the dissociation rate constant k increases stepwise when a new product channel ($J=1.5$) opens. In the RRKM theory, a reaction rate constant k is expressed as

$$k = W/h\rho, \quad (7)$$

where W is the number of states in the transition state (TS), ρ is the density of states of the reactant and h is Planck's constant. If there is no barrier on the potential surface of NO₂ along the dissociation coordinate, it can be said that the TS is located at infinite distance, i.e., the TS is very close to the product state and is regarded as a "loose complex" in which the NO fragment rotates freely. If this loose complex picture holds, W may be easily calculated by counting the number of channels by PST; $W=4$ and 8 for $J=0.5$ and $J=1.5$, respectively, in the case of $J_{\text{NO}_2} = 0.5$, and $W=8$ and 14 for $J=0.5$ and 1.5 , respectively, in the case of $J_{\text{NO}_2} = 1.5$. Since ρ can be treated as a constant in the narrow energy range of $\sim 13 \text{ cm}^{-1}$, k is proportional to W . Therefore, when the new channel with $J=1.5$ of NO opens, W increases stepwise and, consequently, k increases stepwise.

To obtain an absolute value of k , it is necessary to estimate ρ . It is in general difficult to derive ρ experimentally in the high energy region where the dissociation reaction occurs. Therefore, a crude estimation such as the Whitten–Rabinovich approximation is often adopted to predict ρ . However, in the present case, ρ can be obtained from the observed peak density in the LIF spectrum of the parent NO₂ just below the dissociation limit. The observed peak density in the energy region between -5.0 and 0.0 cm^{-1} is $8.2 \text{ level/cm}^{-1}$. Considering that (i) the $R(0)$ transition splits into two components representing $J_{\text{NO}_2} = 0.5$ and 1.5 , and (ii) an individual peak represents one transition to a vibronic level, the density of vibronic levels is $4.1 \text{ levels/cm}^{-1}$. Since J is a good quantum number, the two vibronic sequences with $J_{\text{NO}_2} = 0.5$ and $J_{\text{NO}_2} = 1.5$ should be treated separately, and $\rho = 4.1 \text{ levels/cm}^{-1}$ should be used for both $J_{\text{NO}_2} = 0.5$ and 1.5 . In Fig. 5, the calculated values of k obtained by using Eq. (7) are shown as horizontal lines. In the region where only the $J=0.5$ channel is open, $k = 2.9 \times 10^{10}$ and $5.8 \times 10^{10} \text{ s}^{-1}$ are obtained for $J_{\text{NO}_2} = 0.5$ and 1.5 , respectively. Since ρ is common for $J_{\text{NO}_2} = 0.5$ and 1.5 , PST predicts that k for

$J_{\text{NO}_2} = 1.5$ is twice as large as that for $J_{\text{NO}_2} = 0.5$ in the region where only $J=0.5$ is energetically possible. On the other hand, if K mixing occurs in the highly excited energy region via a rovibronic interaction, the selection rule $\Delta K=0$ is broken and the number of observed transitions for $J_{\text{NO}_2} = 1.5$ becomes larger than for $J_{\text{NO}_2} = 0.5$. If one assumes complete K mixing, the number of detectable states for $J_{\text{NO}_2} = 0.5$ is doubled and that for $J_{\text{NO}_2} = 1.5$ is quadrupled. Therefore, ρ for $J_{\text{NO}_2} = 1.5$ becomes exactly twice as large as ρ for $J_{\text{NO}_2} = 0.5$ and then k is calculated to be $4.3 \times 10^{10} \text{ s}^{-1}$ for both $J_{\text{NO}_2} = 0.5$ and 1.5 . Previously, evidence for rovibronic interaction in excited NO₂, which causes the K mixing, was reported by Lehmann and Coy²⁷ and by Delon *et al.*²⁸ for the energy regions $\sim 16\,810$ – $17\,100$ and $16\,500$ – $18\,500 \text{ cm}^{-1}$, respectively.

In general, a rate constant k calculated by PST is larger than the observed value, so that PST is regarded as the theory which gives only an upper limit of the rate constant.²⁹ In PST, it is assumed that all of the angular momenta involved in the reaction process are spatially isotropic, and as a consequence, all m sublevels are equally populated. In other words, in PST the only assumption about the angular momenta is their conservation expressed by Eq. (4) and no correlation among angular momenta is taken into account. However, recent studies on the photodissociation processes have revealed that the angular momentum distribution of the fragment is often anisotropic.³⁰ Under these circumstances W should become smaller than the PST value. Indeed, as shown in Sec. III D, in the photodissociation of NO₂, the alignment effect of J is also observed clearly. The magnetic sublevel M is preferentially populated in $|M|=J$. This anisotropy may reduce W and, consequently, the rate constant k . Though K may be strongly mixed in the excited state, in some cases K mixing may not be too strong and the $K=0$ level of NO₂ may be selectively excited. This K selection of NO₂ may also restrict the angular momentum distribution. Though this type of restriction has not been discussed so far, it is not surprising that the selection of K induces an anisotropy in the angular momenta in the photodissociation process, since this selection means a particular orientation of J with respect to the parent molecule.

As discussed in Sec. III B, it can be assumed that all $R(0)$ transitions of NO₂ split into two fine-structure components $J_{\text{NO}_2} = 0.5$ and 1.5 . Delon *et al.*²⁸ showed that the fine-structure splitting scatters largely in the $16\,500$ – $18\,500 \text{ cm}^{-1}$, but it seems that most of these splittings are less than 0.1 cm^{-1} . Though spin–rotation constants near the dissociation threshold are not known, some splittings may be smaller than the laser resolution of 0.05 cm^{-1} and the density of vibronic levels ρ may be larger than the observed level density of $4.1 \text{ levels/cm}^{-1}$. Furthermore, it is possible that all of the levels do not appear as detectable transitions in the LIF spectrum, i.e., some levels whose intensities are smaller than the signal-to-noise (S/N) ratio may be missed and ρ may be underestimated.

Very recently, Brucker *et al.*²⁵ measured the dissociation rate constant of NO₂ in the excess energy region be-

tween 0 and 800 cm⁻¹ in the time domain by using a picosecond laser. They reported that the dissociation rate constant increases stepwise at excess energies of 100 and 220 cm⁻¹, and the energy intervals of 100 and 120 cm⁻¹ are ascribed to a bending mode frequency of NO₂ in the transition state. However, this “tight” transition state inferred in their study contradicts the “loose” transition state we propose here. If a loose complex is assumed, the step observed at ~100 cm⁻¹ in their experiment may be due to an opening of a new channel of NO (²Π_{3/2}) which is higher in energy by 119.7 cm⁻¹ than NO (²Π_{1/2}). The smallest rate constant 1.6 × 10¹¹ s⁻¹ in their experiment just above the dissociation limit is almost 20 times larger than our value of $k = 8.5 \times 10^9$ s⁻¹. This inconsistency is probably due to the fact that a number of eigenstates of NO₂ are pumped in their experiment by a short time laser whose spectral bandwidth is 20–80 cm⁻¹. When the picosecond laser is tuned to the dissociation threshold, the laser with a broad bandwidth excites NO₂ into many eigenstates simultaneously, and thus, an average value of the rate constants for these eigenstates is obtained. Therefore, the value may roughly correspond to a rate constant of eigenstates located at 0–80 cm⁻¹ above the dissociation limit. By using the smallest rate constant $k = 8.5 \times 10^9$ s⁻¹ determined in our experiment in the energy region where only one dissociation channel $J = 0.5$ opens, and the number of states counted by PST, the rate constant at the excess energy of 80 cm⁻¹ is calculated to be $k = 1.1 \times 10^{11}$ s⁻¹, which is in good agreement with $k = 1.6 \times 10^{11}$ s⁻¹ derived by the picosecond laser experiment. In the present study, we clearly show that the rate constant increases stepwise when a new rotational channel opens. Such a variation of the rate constant in a narrow energy region can be investigated only through measurement in a frequency domain experiment.

C. Rotational and Λ doublet component distribution of NO

Previous photodissociation studies³¹ showed that when a diatomic fragment has a Λ doublet, one of the components of the Λ doublet is often preferentially produced. In the high J limit, a lobe of the wave function of an unpaired electron of the A'' level orients perpendicularly to the rotation plane of a diatomic fragment, and that of the A' level is located on the plane. The preference of one component of the Λ doublet to the other has been ascribed to the conservation of electronic symmetry in the dissociation process, i.e., the electronic correlation between the parent molecule and the diatomic fragment prefers the same Λ component over the other for all J . However, such a preference rule cannot be found in the Λ doublet component distribution observed in the present study. As shown in Fig. 8, at the same photolysis energy, the A' component is preferred for some J 's and the A'' component for other J 's, and it seems that there is no rule in preference of the two Λ doublet components. Each Λ doublet component also has parity “+” or “-”, i.e., the A' and A'' components have “+” and “-”, respectively, for $J = 0.5, 2.5, \dots$, and “-” and “+”, respectively, for $J = 1.5, 3.5, \dots$. Bigio and Grant³² reported some correlation between the parity of

parent NO₂ and the parity of fragment NO (²Π_{1/2}) just above the dissociation limit to NO (²Π) + O (¹D). However, in the present study, there is no preference of one parity over the other as shown in Fig. 8.

It may be possible to explain the observed fluctuation of the J distribution in each Λ doublet by the Franck–Condon principle, i.e., the J distribution is determined by the overlap of the wave function of the parent molecule with that of the final state. The product state distribution is given as a probability of finding a wave function of the final state in the initial wave function of the parent molecule. This treatment was applied successfully to predict the rotational distribution of the fragment specific to the photodissociation process.^{33,34}

In the photodissociation of H₂O by Häsler *et al.*,³⁵ H₂O is excited to a single rotation–vibration level using an IR laser and is subsequently photodissociated by an ArF laser at 193 nm. The distribution of the fragment OH exhibits significant fluctuations in both the rotational and Λ doublet components, which is similar to that observed in the present study. In order to interpret their results, they adapted the Franck–Condon principle including the Λ doublet of the fragment for the first time and could successfully reproduce the observed oscillatory distribution. Reflecting the small bending quanta of H₂O, the fragment OH is preferentially populated in low J levels. Though it is not shown in their calculation, it seems that the J fluctuation disappears if the two Λ doublet components having the same J are averaged.

In the case of NO₂, it may also be appropriate to apply the Franck–Condon principle including the Λ doublet in order to explain the fluctuations of the rotational population in each Λ doublet component of NO, though H₂O dissociates via a direct dissociation process and NO₂ dissociates via a vibrational predissociation. Since NO₂ predissociates through quasibound states, an overlapping of the wave function of a *quasibound state* with that of a final state must be considered. However, at the present stage, it is practically impossible to know the exact eigenfunction of these quasibound states which are extremely highly excited in vibration. Thus, the observed fluctuation of the population ratio among the rotational states and Λ doublets is discussed only in a statistical treatment in Sec. IV D.

D. State-to-state reaction vs statistical reaction

For the dissociation reaction which proceeds on a potential energy surface with a barrier, the RRKM theory can predict a rate constant for the reaction, but it cannot predict the product state distribution of the fragments. Usually the product state distribution is determined by the dynamics on a steep potential energy surface after the TS. In the case of NO₂, the potential energy surface along the dissociation coordinate has no barrier and the TS is located at infinite separation of the fragments. If each state in the TS is connected adiabatically to one rotational state of the NO fragment, the population at one rotational state must be proportional to a partial rate constant for one reaction channel divided by the total rate constant. Therefore, the observed fluctuation in the product state distribution

means a fluctuation in a partial rate constant. This fluctuation, which can be directly related to the state specificity, has been often interpreted as a consequence of incompleteness of the intramolecular vibrational energy redistribution (IVR).

An alternative explanation of the observed state specificity was proposed by Polik *et al.*^{7,8} and Miller *et al.*⁹ to interpret the large fluctuations of the rate constant observed in the photodissociation of D₂CO. They determined the dissociation rate constants for respective eigenstates of highly excited D₂CO by using Stark level crossing spectroscopy.⁷ Though the observed rate constants fluctuate by three orders of magnitude, their average value is consistent with a statistical calculation by the RRKM theory including a tunneling effect. Based on the distributions of the level spacings and the S₀-S₁ matrix elements, both of which support complete IVR, they inferred that the rate constant is proportional to the square modulus of the overlap of the wave function of an activated state with that of a transition state using Fermi's golden rule, and showed that the rate constants fluctuate as a necessary consequence of complete mixing of vibrational levels of D₂CO.^{8,9}

The vibrational dynamics of NO₂ is said to be already chaotic even in the low energy region.²⁸ Recently, we measured the vibronic level structure with high resolution just below the dissociation threshold.³⁶ The nearest-neighbor level spacing distribution is found to be of a Wigner type and a correlation hole is clearly found in the Fourier transform of the spectra. Furthermore, the intensity distribution is well-represented by a χ square distribution. These results suggest that (i) there is a strong correlation among the vibronic levels near the dissociation limit, indicating complete mixing of the three vibrational modes, and (ii) a state-dependent partial rate constant observed in the photodissociation of NO₂ is interpreted as a quantum fluctuation as proposed by Polik *et al.*^{7,8} and Miller *et al.*⁹ In the case of D₂CO, the derived rate constant is a total rate constant K , which is defined as a summation of partial rate constants

$$K = k_1 + k_2 + k_3 + \cdots + k_n, \quad (8)$$

where k_i represents a partial rate constant for the i th channel. When k_i independently obeys a χ square distribution with one degree of freedom, K fluctuates by a χ square distribution with n degrees of freedom. Therefore, the degrees of freedom, which are derived by comparing the observed distribution of the rate constant with a theoretical χ square distribution, can be regarded as the number of channels in the transition state.

In the present study, the ratio of a partial rate constant k_i to the total rate constant K can be derived from the observed PHOFEX spectrum. As the number of dissociation channels increases, the degrees of freedom for the χ square distribution of the total rate constant K increases according to Eq. (8) and equivalently the fluctuation in K decreases. However, when each partial rate constant is observed, the fluctuation of the distribution of each partial rate constant may be seen even in the region where W is considerably large. The rate constant equation of the

RRKM theory [Eq. (7)] can be rewritten as $\Gamma/\Delta E = W/2\pi$, where Γ is the homogeneous linewidth and ΔE is a mean level spacing. When $W \gg 2\pi$, many eigenstates of the parent molecule overlap with each other and it is impossible to discriminate a dissociation rate for one eigenstate from those of other adjacent eigenstates.

In the case of dissociation on a potential energy surface with a barrier, the TS must be tight and the vibrational frequencies of the TS are relatively large in general, and consequently W is small up to a relatively high excess energy region. However, in the case of the dissociation of a triatomic molecule on a potential energy surface without a barrier, the TS is loose and the frequency of its vibration, i.e., internal rotation, is very low, so that W becomes large very rapidly as the excess energy increases and broadened peaks overlap each other significantly. This means the fluctuation decreases more rapidly in the case of dissociation on a potential energy surface without a barrier than with a barrier. Nevertheless, the fluctuation of the product state distribution in the photodissociation of NO₂ still persists even in the higher energy region where $J=30$ of NO ($v=0$) is energetically allowed.¹⁴ In this region, W calculated by PST is more than 600 and $\Gamma/\Delta E \approx 100$, indicating that about 100 states are mixed. It may be possible that many more levels are necessary to realize a completely state-independent reaction, or that there is another origin for the observed fluctuation.

Last, although the rotational state distribution is statistical on average, a significant population inversion is observed in the vibrational distribution where vibrational excited NO is energetically allowed.^{11,12} This vibrational state distribution could not be explained by statistical theories. In contrast to the rotational state distribution, there may be some kinds of restrictions such as adiabaticity in vibration for the vibrational excitation of NO.

V. SUMMARY

In this study, the photofragment excitation (PHOFEX) spectra of NO₂ are observed by monitoring the specific quantum states of fragment NO (${}^2\Pi_{1/2}; v=0, J=0.5-6.5$) in the energy region 0-160 cm⁻¹ above the dissociation limit to NO (${}^2\Pi_{1/2}$) + O (3P_2). An extremely cold (~ 1 K) parent NO₂ in a supersonic jet and a high resolution (~ 0.05 cm⁻¹) photolysis laser make it possible to prepare quasibound eigenstates of NO₂ just above the dissociation limit.

The main results are as follows:

(1) Dissociation thresholds for each rotational state of NO are consistent with energies predicted from the corresponding rotational energies of a free NO molecule. This observation indicates that the dissociation proceeds on a potential energy surface without a barrier.

(2) The dissociation rate constant is obtained from the peak width of the PHOFEX spectrum and the smallest rate constant is $k=8.5 \times 10^9$ s⁻¹ in the energy region, where only $J=0.5$ of NO is energetically allowed. When a new product channel $J=1.5$ opens, the rate constant increases stepwise. This implies that the transition state is a

loose complex, which justifies the calculation of the state number in the transition state by the phase space theory.

(3) At fixed photolysis energies, the observed rotational product state distribution of NO in each of the two Λ doublet components fluctuates significantly. When the two components of the Λ doublet having the same J are averaged, this fluctuation decreases largely, but still remains around the value predicted by phase space theory. Based on a strong correlation among eigenstates revealed by the statistical analyses of the vibronic levels observed in the LIF spectrum below the dissociation limit, the state specificity in the photodissociation process is explained by a quantum fluctuation due to the complete intramolecular vibrational energy redistribution (IVR) in the parent NO₂.

ACKNOWLEDGMENTS

The present work is supported in part by a Grant-in-aid for Scientific Research (No. 02403006). J. Miyawaki thanks the Japan Society for Promotion of Science for a fellowship for Japanese junior scientists (No. 1141). We are grateful to Dr. E. A. Rohlffing for sending to us copies of two papers on laser-induced grating spectroscopy of NO₂ prior to their publication.

¹F. F. Crim, *Science* **249**, 1387 (1990).

²For example, P. J. Robinson and K. A. Holbrook, *Unimolecular Reactions* (Wiley, London, 1972).

³B. R. Foy, M. P. Casassa, J. C. Stephenson, and D. S. King, *J. Chem. Phys.* **90**, 7037 (1989).

⁴X. Luo and T. R. Rizzo, *J. Chem. Phys.* **96**, 5129 (1992).

⁵Y. S. Choi and C. B. Moore, *J. Chem. Phys.* **97**, 1010 (1992).

⁶H. -L. Dai, R. W. Field, and J. L. Kinsey, *J. Chem. Phys.* **82**, 1606 (1985).

⁷W. F. Polik, D. R. Guyer, and C. B. Moore, *J. Chem. Phys.* **92**, 3453 (1990).

⁸W. F. Polik, D. R. Guyer, W. H. Miller, and C. B. Moore, *J. Chem. Phys.* **92**, 3471 (1990).

⁹W. H. Miller, R. Hernandez, C. B. Moore, and W. F. Polik, *J. Chem. Phys.* **93**, 5657 (1990).

¹⁰D. K. Hsu, D. L. Monts, and R. N. Zare, *Spectral Atlas of Nitrogen Dioxide 5530 to 6480 Å* (Academic, New York, 1978).

¹¹H. Zacharias, M. Geilhaupt, K. Meier, and K. H. Welge, *J. Chem. Phys.* **74**, 218 (1981).

¹²H. Zacharias, K. Meier, and K. H. Welge, in *Energy Storage and Redistribution in Molecules*, edited by J. Hinze (Plenum, New York, 1983).

¹³M. Mons and I. Dimicoli, *Chem. Phys.* **130**, 307 (1989).

¹⁴D. C. Robie, M. Hunter, J. L. Bates, and H. Reisler, *Chem. Phys. Lett.* **193**, 413 (1992).

¹⁵U. Robra, H. Zacharias, and K. H. Welge, *Z. Phys. D* **16**, 175 (1990).

¹⁶J. Miyawaki, K. Yamanouchi, and S. Tsuchiya, *Chem. Phys. Lett.* **180**, 287 (1991).

¹⁷R. E. Smalley, L. Wharton, and D. H. Levy, *J. Chem. Phys.* **63**, 4977 (1975).

¹⁸T. C. Hall, Jr. and F. E. Blacet, *J. Chem. Phys.* **20**, 1745 (1952).

¹⁹*Handbook of Chemistry and Physics*, 62nd ed., edited by R. C. Weast (CRC, Boca Raton, FL, 1981).

²⁰T. J. Butenhoff and E. A. Rohlffing, *J. Chem. Phys.* **98**, 5460 (1993).

²¹C. E. Moore, *Atomic Energy Levels* (Natl. Stand. Ref. Data. Ser. Natl. Bur. Standan. U.S. Government Printing Office, Washington, D. C. (1971), No. 35).

²²*Molecular Spectra and Molecular Structure*, edited by K. P. Huber and G. Herzberg (Van Nostrand-Reinhold, New York, 1979), Vol. 4.

²³C. H. Greene and R. N. Zare, *J. Chem. Phys.* **78**, 6741 (1983).

²⁴G. E. Hall, N. Sivakumar, and P. L. Houston, *J. Chem. Phys.* **84**, 2120 (1986).

²⁵G. A. Brucker, S. I. Ionov, Y. Chen, and C. Wittig, *Chem. Phys. Lett.* **194**, 301 (1992).

²⁶P. Pechukas and J. C. Light, *J. Chem. Phys.* **42**, 3281 (1965).

²⁷K. K. Lehman and S. L. Coy, *J. Chem. Phys.* **83**, 3290 (1985).

²⁸A. Delon, R. Jost, and M. Lombardi, *J. Chem. Phys.* **95**, 5701 (1991).

²⁹For example, W. L. Hase and R. J. Duchovic, *J. Chem. Phys.* **83**, 3448 (1985).

³⁰G. E. Hall and P. L. Houston, *Annu. Rev. Phys. Chem.* **40**, 375 (1989).

³¹M. A. Alexander *et al.*, *J. Chem. Phys.* **89**, 1749 (1988), and references cited therein.

³²(a) L. Bigio and E. R. Grant, *J. Phys. Chem.* **89**, 5855 (1985); (b) *J. Chem. Phys.* **87**, 360 (1987).

³³A. Ogai, C. X. Qian, and H. Reisler, *J. Chem. Phys.* **93**, 1107 (1990).

³⁴R. L. Miller, S. H. Kable, and P. L. Houston, *J. Chem. Phys.* **96**, 332 (1992).

³⁵D. Häusler, P. Anderson, and R. Schinke, *J. Chem. Phys.* **87**, 3949 (1987).

³⁶J. Miyawaki, K. Yamanouchi, and S. Tsuchiya (unpublished).